Microscale Wireless Electrical Stimulators for Electroceutical Applications: a Review

Chae Eun Lee[1], Yu Ri Kim, Joon Young Lim and Yoon Kyu Song[a]
Graduate School of Convergence Science and Technology, Seoul National University
E-mail : [1]celee1025@snu.ac.kr

***Abstract* - Electroceutical has been used as an attractive approach to disease treatment, using electrical stimulation to modulate metabolic function and restore body homeostasis. As the first generation of electroceuticals, cardiac pacemakers and implantable defibrillators have saved countless lives over several decades. Due to the remarkable technological progress of implantable medical systems over the past few years, it has reached the point of transforming the existing system into a micro-scale system using semiconductor microelectronics. Herein, research trends regarding various disease applications of electroceuticals are reviewed. In particular, the components, specifications, and circuit structures of the stimulation sub-systems in electroceuticals are thoroughly analyzed.**

***Keywords*—Distributed microsystem, Electroceutical, Electrical stimulation, Implantable system, Microstimulator**

I. INTRODUCTION

Electroceutical, derived from electronics and pharmaceuticals, has been used to treat diseases by regulating the body's natural healing mechanism through electrical stimulation of the nervous system. First-generation electroceuticals, which are cardiac pacemakers, defibrillators, cochlear implants, and deep brain stimulators, have helped improve the quality of life of numerous patients for decades.

Electroceutical has the advantage of having fewer side effects by stimulating only a specific target organ. It eliminates the inconvenience of taking medicine every day and maintains the result for a long time. Hence, the treatment cost is lower than medicine that is purchased periodically.

Researchers at the University of Wisconsin developed an implantable system to reduce food intake and control weight after stimulation of vagus nerve afferent fibers [1]. Researchers at Tohoku Medical University reported that it could promote regeneration of damaged liver by activating FoxM1 through vagus nerve stimulation [2]. Wuhan University, China, published a study showing that vagus nerve stimulation using implantable high-performance hydrogel nanogenerators (HENG) inhibits pro-inflammatory cytokines [3]. According to an animal model experiment in [4], Cristin Welle's group at the University of Colorado announced that it could improve motor function learning during vagus nerve stimulation [4]. Researchers at the University of Pittsburgh have confirmed that vagus nerve stimulation has a potential therapeutic effect on cardiovascular, cerebrovascular, metabolic and depression, and mortality [5]. Since research to use electroceuticals for various target diseases has been actively reported, the related market size will grow further.

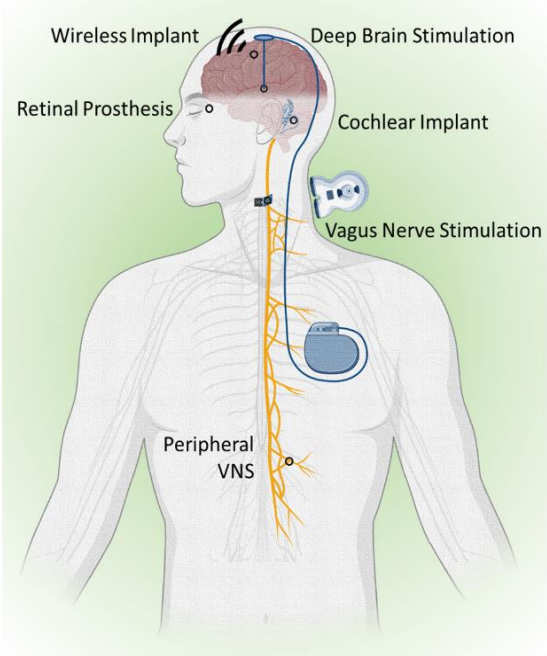

Fig. 1. Clinical electroceuticals widely investigated.

Estimating how electroceuticals will play a significant role in therapeutic medicine depends on an accurate understanding of the link between nerves, organs, and diseases. Equally important, however, are technological advances in implantable electronics. Unlike the studies on the stimulation devices, most electroceuticals are still in their prototype stages. Issues such as size, usability, the lifetime of the battery, and lack of long-term implantable technology still need to be addressed to enhance the usability and functions of these devices for practical use.

a. Corresponding author; songyk@snu.ac.kr

Manuscript Received May. 13, 2022, Revised Jun. 24, 2022, Accepted Jun. 27, 2022

In this study, we comprehensively explain the stimulation methods associated with pre-clinical data and circuit-level detail in implementing the stimulator. These, as shown in Fig. 1, include clinical nerve implants such as cochlear implants to restore hearing [6], [7], retinal prosthesis to restore vision [8], heart failure [9], deep brain stimulator (DBS) for the treatment of movement disorders [10], [11], and pharyngeal and peripheral nerve stimulation to help with dysphagia and gait disorders. Recent electroceuticals include electrical stimulation of the vagus nerve, which modulates the immune system to prevent epileptic seizures [5], relieves rheumatoid arthritis [12], treats heart failure [13], and treats inflammatory bowel disease and intestinal motility disorders [14]. It also includes the hypothesis that electroceuticals may improve memory and consciousness against depression and dementia [15].

In section II, we describe the basic concept of electrical stimulation. In Section III, we report detailed information about stimulation circuit design and define our considerations and results in producing a retinal stimulator. Sections IV deal with the challenges and advantages of distributed microstimulators. Finally, we comment on the overall review of designing a microstimulator and applying it to clinical experiments.

II. ELECTRICAL STIMULATION AS ELECTROCEUTICAL

Clinical research has utilized commercial stimulation devices with FDA approval to improve disease severity or suppress abnormal nerve activity, such as seizures. Clinical stimulators depict different stimulation architectures considering electrodes and tissue environments for optimal performance to the target disease. As shown in Fig. 2, the amount of charge and injection methods differ, which correlates to the electrode's type and size and the target tissue's characteristics. Since the area to the point refers to the injected charge, the graph shows the average amount of charge needed for AP activation. The stimulation charge of electroceutical is relatively low when directly delivering stimulus to nerve cells. In contrast, when a specific area needs constant stimulation using a relatively large electrode, the overall charge density is lowered, and the amplitude increases because it spreads widely.

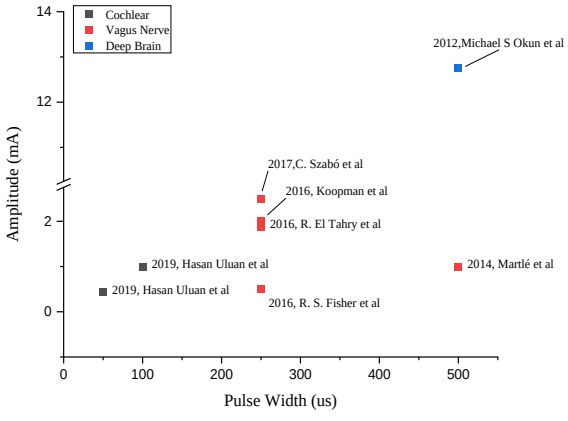

Fig. 2. Commercial stimulation devices and stimulation parameter comparison used in clinical trials

For instance, cochlear implants at the left bottom side bypass the sensory hair cells and directly stimulate the auditory nerve to restore auditory perception. In stimulation, each parameter is related to sound components—usually, the greater the charge, the louder the sound to the patients. Unlike cochlear targeting auditory nerve cells, DBS uses a considerably large electrode to stimulate target tissue. By inserting electrodes into the abnormal part of the brain and giving electrical stimulation, abnormal neural circuits are controlled by DBS, and abnormal movement symptoms are improved. In particular, nerves distributed over a wide area like Vagus nerves have different stimulation methods depending on their use and location. Even if the same amount of charge is applied, there is a difference in applying stimulus in a short time or applying an appropriate amount for a long time.

The generation of an action potential in neurons through electrical stimulation is achieved by delivering a sufficient charge to its membrane. As the excess charge accumulates outside the cell membrane, a potential reversal occurs, triggering an action potential (Fig. 3). Therefore, the energy efficiency of electrical stimulation is highly dependent on the generated voltage and current waveforms and the electrodes' characteristics.

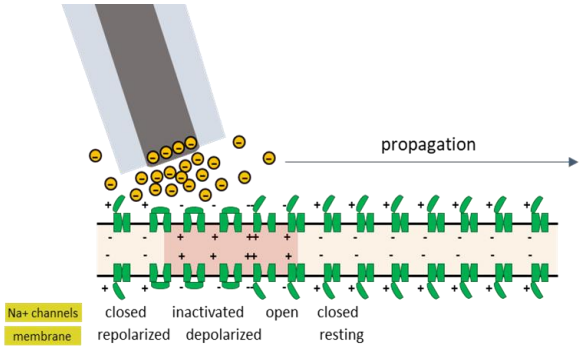

Fig. 1. Electrical stimulation topology at the electrode-tissue interface

The waveform is determined based on the circuit structure of the output stage and the form of the electrode combined. Electrode connections in a monopolar and a bipolar configuration are widely used in standard physiological experiments. Both formats have all the pros and cons in the application, hence selected based on their purposes. The bipolar configuration needs pairs of electrodes and stimulates a limited area while exhibiting a greater compliance voltage because of the circuit structure. The electrode's size and impedance must also be considered prior to the electrode configuration. Size should be small enough compared to the neural cells (~10 μm) to ensure selective stimulation and charge density, while impedance should be low enough to permit effective stimulation. The charge density is determined by the amount of the charge executed and the apparent area of the electrode interface. Conventionally, if the size of the electrode interface reduces, the impedance and the load on the stimulator increase. Therefore, it is vital to find a suitable compromise between them.

After determining the stimulation architectures, neural stimulation has been achieved by either constant-voltage (CV) or constant-current (CC) waveforms from electrical stimulation devices. CV was used in medical devices in the past due to its simple structure, but as a result of clinical trials, patients preferred and experienced greater satisfaction and pain relief with CC stimulation than with CV stimulation [16], [17]. Compared to the same results, CC stimulation has the advantages of better controllability of the amount of charge delivered during stimulation, the accuracy of calibration, and stimulation efficiency so that dominantly used. Also, the CC stimulator is believed to provide a fixed charge regardless of the impedance variation of electrode-tissue interfaces. Research in [18] presented a current-controlled stimulator delivering adiabatic waveforms that is fully-integrated on-chip with no external components necessary to achieve efficient, single-step waveform synthesis.

The CC stimulator also has its drawbacks. A current mismatch causing a charge imbalance is easily observed in the output stage. Moreover, even if the amount of charge reached is calculated through impedance modeling, the ideal value is affected by environment variables before going neurons. Recent studies showed strategies to address this issue in addition to primary stimulation IC.

III. CIRCUIT IMPLEMENTATIONS

Stimulator ICs typically comprise three main parts to fulfill their functionality; a DAC to directly modify the amount of charge supplied from a current source, an output pulse driving stage connected to the electrodes for stimulation, and a digital logic that controls the switches of the connected analog backend according to the digital input command. With these three parts integrated, the desired pulse shape could be obtained by adjusting the waveform parameters, as shown in Fig. 4. Also, complementary circuits are requested for stimulator IC to work as fully implantable electroceuticals. These are wireless power transmission circuits, circuits that could detect optical and chemical changes, electrical signal recording/stimulation, and communication technology

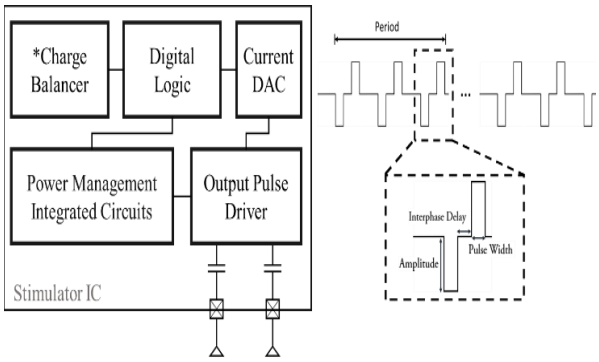

Fig. 3. Block diagram of stimulator IC.
*Charge balancer is optional for primary stimulator IC

A. Digital to Analog Converter

Conventionally, current source designs with voltage DAC connected to voltage to current converter were used, where the converted voltage determines the voltage amplitude of the pulse [19], [20]. However, the current-mode technique has the primary advantages of high-speed, low voltage potential. Current DACs in the stimulator analog backend are usually correlated to the digital controller, which programs stimulus pulse parameters (including pulse width, amplitude, and frequency). Each transistor works as a current source, and analog switches are connected to a summing point and control the ratio of the current flowing through the point. Most devices use the current steering DACs where the output current is multiplied or mirrored to the output stage, as shown in Fig. 5(a). It is preferred because of its small size, simplicity, high resolution, and fast conversion speed [21]. Based on the binary principle, binary-weighted structures are applied to current sources, as in Fig. 5(b). The number of bits that determine the stimulation pulse amplitude sets the resolution of DAC. Therefore, DAC topologies and sizes are chosen based on their purpose and characteristics.

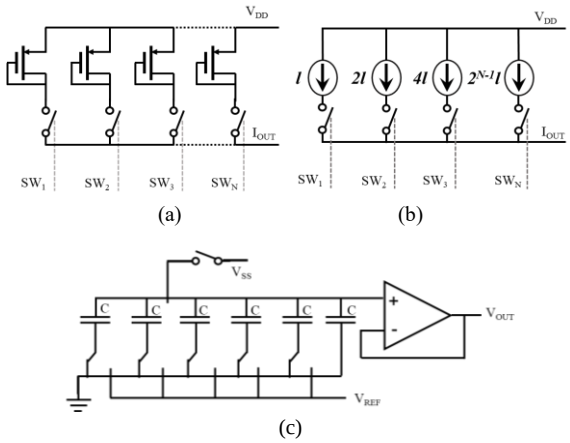

Fig. 2. Simplified schematics of DACs. (a) Current steering DAC, (b) Binary weighted current steering DACs, (c) Capacitive DACs.

For instance, we applied a 5-bit binary-weighted current steering DAC for the current source. Given the operation speed of the retinal prosthesis, a fast on/off switching speed is crucial. The PMOS analog switches placed on each stage are controlled by a digital controller. With a 10 μA reference current, the maximum summed-up current was 310 μA. Also, a multi-channel system's relatively low stimulation current and high spatial resolution prefer current DAC with a small IC area.

The area should be a concern considering that the matching and parasitic components determine the accuracy of the current source. In addition to the DAC topology, various attempts are proposed to reduce the area and increase the efficiency of the floor plan guaranteeing performance. Sharing the DAC is widely used in multi-channel systems [22], [23] or bidirectional systems with recording circuits integrated. Capacitive DACs (in Fig. 5(c) are typically found primarily in SAR ADCs at the neural recording stage in neural interface integration systems [24], sharing them to provide a compact design with low power consumption.

Meanwhile, the linearity and the minimum mismatch of each LSB and MSB in DAC are always considered low power consumption. Linearity of the DAC is affected by the current output stage that follows, and as the number of channels of the stimulator increases, errors due to power distribution and simultaneous control exist. To deal with the issue, creating power isolation of each channel with switch capacitors was attempted in [25]. The study in [26] presented a 10-bit capacitor-charge time-based DAC (CT-DAC) as a revision of the conventional current-mode DAC that uses microamps for biasing and offers high resolution with simple layout requirements with low power consumption.

B. Stimulation Output Stage

The circuit that plays a significant role in determining the characteristic of the stimulator is the output pulse generation stage. The stimulation output stage delivers a monophasic, biphasic, or arbitrary-waveform current to the electrode-tissue interface. The interface is modeled into a serial impedance known as load(Z) (Fig. 6(a). The findings that the load impedance increases over time because of the electrical reaction between the electrode and electrolyte during stimulation and scar tissue adhesion after implementation shows that the output stage endures large ranges of load impedances. With higher compliance voltage, the current driver can supply a broader range of currents to a given load. On circuit design, it is conventionally difficult to generate the large compliance voltages necessary to support constant-current stimulation across the load. For the large compliance voltage, transistor stacking output current driver is typically used with HV generation circuits such as charge-pump [27], [28], or HV output stage with OP Amp [26]. For instance, the pulse frequency modulation (PFM) feedback network in [29] implemented the stimulation pulse generator, which digitally controls the charge pump to generate a dynamic supply voltage to the output stage of four stacked transistors. There was an attempt to lower the risk of using the HV output interface by putting the HV protective switch [30]. However, high voltage supplies and current sources in an HV process may lead to poor power and area efficiencies. Therefore, maximizing the output impedance of the stimulator lets well-controlled constant current under variable load conditions. As for increasing the output impedance of the stimulator, output stages are proposed in various structures, such as using a modified regulated cascoded current mirror [31] and customized output current source [22].

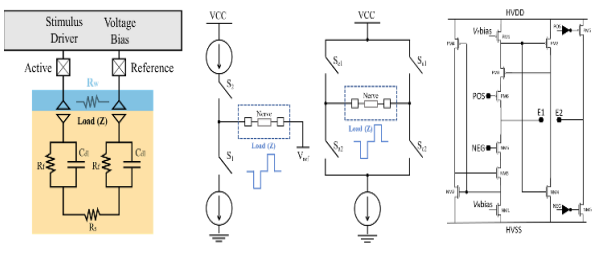

Fig. 4. Schematics of stimulation output stage driving biphasic pulse. (a) Load impedance model of the electrode-tissue interface. (b) Current source-sink model. (c) Current source H-bridge model. (d) High output impedance current output stage

C. Circuits for Charge-Balanced Stimulation

Charge balanced stimulation gain attention for prohibiting nerve damage due to electrochemical reactions, pH changes, gas formation, and excessive production of toxic by-products from electrode dissolution [32]. However, the imbalance charge results from different reasons. Various things include unequal pulse shapes, imbalances and mismatches in the current source, and DC voltage due to the residual charge.

It is well known that a biphasic pulse guarantees a balanced charge injection. Generally, two approaches are employed to generate the biphasic current pulse: a source-sink current driver (Fig. 6(b) and an H-bridge topology (Fig. 6(c). The source-sink model dual supplies stimulation with a single current driver providing desired current to each phase respectively [30], [33]–[35]. Mostly, current steering DACs are combined as current sources. H-bridge topology is employed to produce a biphasic pulse from a single current source, intended to reduce the mismatch between phases [36]–[38].

Regarding the retinal prosthesis, we tried to increase the output impedance of the output pulse generator. Retinal prostheses are applied to high-density retinal ganglion cells and require smaller electrodes for higher spatial density. As shown in Figure 6d, the current source-sink driver is modified with a regulated cascode current mirror. The feedback allows the current mirror output stage to withstand impedance changes of up to 40 kΩ. Biphasic pulses from active electrode E1 are guided by reference electrode E2.

The monophasic cathodic pulses are efficacious in generating a desired neural reaction (action potential) but create residual charge at the electrode-electrolyte interface causing potential electrode corrosion and tissue damage. In a biphasic current stimulation, mostly the anodic pulse (second phase) neutralizes the excess charge, thus eliminating DC-current flow. Therefore, it is crucial that the cathodic pulse accurately delivers the charge to the tissue, and the anodic pulse compensates for the injected charge. Different stimulation output stages are compared against our design in Table I. The architectures vary along with their applications.

As for the design methods to deliver precise charge-balanced charge injection, many studies have been conducted. Active charge balancing either removes the residual charge on the electrode or controls the output charge. Despite the increase in system size, various techniques have been studied that take advantage of the improvements. In contrast, passive charge balancing is the simplest form of charge balancing. It utilizes a passive in-line capacitor to provide an inverse stimulation pulse to the electrode. These methods have side effects of losing control of precise waveform output. Moreover, since chemically reactive electrolytes surround the exposed environment, the system without the blocking capacitor remains at the risk of waveform distortion.

In the case of the active charge balancing technique, either the stimulation reaction or the charge of the output stage functions as feedback control of the stimulator. Measuring

Table I. Comparisons of the microstimulator

	[45]	[46]	[28]	[40]	[47]	This Work
Stimulation Type	Current controlled (CCS)	Current controlled (CCS)	Current controlled (CCS)	High-frequency, switched-capacitor (HFSC)	Current controlled (CCS)	Current controlled (CCS)
Supply voltage	3.3 V	3.2 V	Adaptive (~3.3 V)	1.8 V	1 V	3.3 V
Voltage compliance	± 6 V	12.8 V_{HV}	6.7 – 12.3 V	5 V	2.5 V	3V
Charge balancing method	Discharge (Electrode shorting)	Modulation (Anodic current modulation & electrode shorting)	Discharge (Electrode shorting)	Discharge (Electrode shorting - active charge balancing)	Passive charge balancing	Modulation (Anodic current modulation)
Current	± 3 mA	1 mA	2.4 mA	34 nC and 120 nC	60 µA – 1.86 mA	40 – 330 µA
Pulse width	60 µs, 10 µs interphase delay	100µs with 20 µs of interphasic	0.5 ms pulse width, 2.5 ms period	2.37 µs clock period	9.5 µs – 304 µs width, 9.5 µs – 304 µs delay	100 µs – 2ms
Target	Parkinson's disease	Universal use	DBS	DBS	Hippocampal CA1, CA3	Retinal Prosthesis
Stimulus configuration	Monopolar biphasic	Bipolar Biphasic	Biphasic	Biphasic	Biphasic	Biphasic
Technology	180nm LV CMOS	180nm standard CMOS	180nm LV CMOS	180nm HV CMOS	130nm standard CMOS	180nm TSMC CMOS

the output voltage of the stimulation is one of the methods widely used. The charge balancing technique in [42] measured the residual voltage after each stimulation phase and adjusted the amplitude of the next anodic current pulse according to the value. In a similar context, the feedback sensor in Fig. 7(a) sends measured voltage to the proportional-integral-derivative (PID) controller, which manipulates the pulse width of each phase. Discharging by pausing the operation is sometimes chosen in active charge balancing. The additional comparator determines whether to shut down the process based on the voltage at the electrode, as shown in Fig. 7(b). Another simulator proposed in Fig. 7(c) used a time-based charge balancing (TBCB) loop to monitor the voltage at the stimulation electrode during the inter-pulse phase. Several other circuit designs demonstrate, such as a high-matching current driver to produce adjustable biphasic current [43] or a programmable charge-balanced neurostimulation waveform synthesizer which enables flexibility in finding optimal neuromodulation paradigms for pathological symptom suppression [44].

Table I describes the overall specifications of the recently investigated microstimulator. As previously mentioned, current-controlled current stimulation is recently preferred. According to the target, different specs of stimulators were designed. Also, due to the emergence of scar tissue and various other physiological components, the impedance of the electrode-tissue interface increases. Accurate charge delivery is essential when the required stimulation charge and the threshold charge density are high

D. Digital Logic

Different neural stimulus parameters improve stimulation performances, minimize energy usage, and decrease side effects with an electrical pulse. Many electrode combinations and stimulus parameter settings (including pulse width, amplitude, and frequency) could be modulated

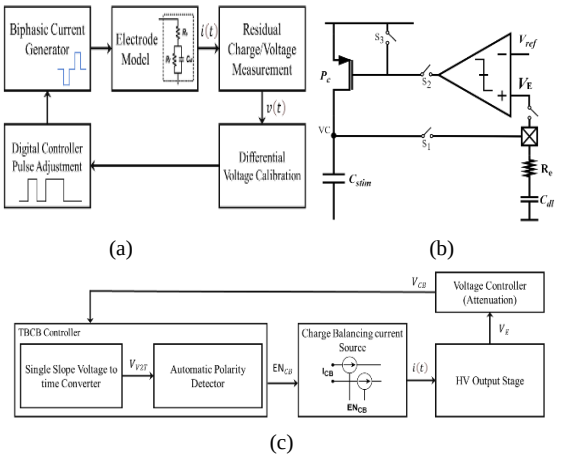

Fig. 5. Conceptual image of various active charge-balancing methods. (a) Proportional-integral-derivative (PID) controller with feedback sensor [39]. (b) Active charge balancing with the comparator. The comparison between the reference voltage and electrode voltage controls the operation of the entire circuitry stops operating [40]. (c) A data processing procedure of time-based charge balancing (TBCB) [41]

by the control output signal of the digital logic.

As the clock and data recovery (CDR) circuit demodulates the RF signal, digital logic interprets the command and controls the stimulation analog backend. Several counters and registers produce the sequential switching signal delivered to the analog switches offering programmable stimulation pulses. The way of decoding the command varies on the parameter range. A lookup table with fixed order is preferred if the designer intentionally wants to adjust only a few variables and simplify the module [48].

On the other hand, when a wide range of stimulation parameters is needed, more extended commands and more registers would increase the size of the design. One thing to be aware of is that if the designer recklessly lengthens the command bit to contain all the modulating commands, the

burden on other circuits increases. A faster clock enables the system to process a more extended order, and a more sophisticated wireless data transceiver is required to reduce the bit loss rate. As a method of decoding a command, there are various things such as relatively simple things such as the Manchester encoding [49], [50]. In particular, we used a 1MHz system clock and the 34-bit serial command. Each data for stimulation parameters is placed after the address bit. A clock divided by 20 kHz resulted in a unit pulse width of 50 μs.

Other than the binary command encoding, various implementations according to the application are suggested. Some clinical researchers implement feedback algorithms in digital logic operating based on their recorded reactions to calibrate stimulus. A research team in [51] modulated the frequency of the stimulation signal using filtering and linear delayed LFP recording to suppress neural oscillations in delayed-feedback high-frequency stimulation.

E. Implantable system

The technological challenge of implantable neural stimulation is to achieve a fully integrated independent stimulation system. Some conditions must be met for application in clinical practice. First, implantable electronic devices should operate for a long time in the physiological environment of the human body, so a very high level of sealing must be maintained for several decades. In addition, to measure nerve signals or stimulate nerves, parts of the system must be electrically exposed to bodily fluids. Second, if the device implanted in the body uses excessive power, the temperature rises, which may cause necrosis of the living tissue around the device or abnormal behavior of surrounding organs. Accordingly, the implantable electronic device should consume very little power. Third, since electrical energy is required to operate all electronic devices, a method capable of safely and continuously supplying sufficient electrical energy is needed for successful implantable electronic devices. Primarily, there is a limit to the rate at which the human body absorbs energy per unit mass when exposed to radio frequencies called the specific absorption rate (SAR) limit.

However, since the stimulation causes instance power consumption while actively giving the stimulus, a stable and high-efficiency power source is essential. Until now, power transmission by batteries or magnetic induction has been the mainstream, but recently, there are energy-harvesting or bio-cells that obtain power from RF electromagnetic waves, light energy, or kinetic energy for ultra-small and ultra-low-power bioelectronic devices.

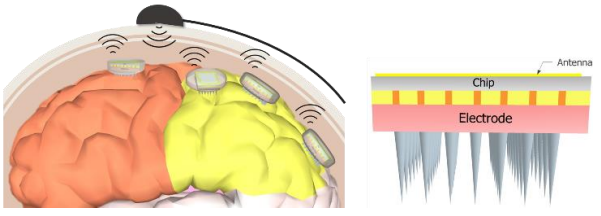

(a) (b)

Fig. 6. Illustration of spatially distributed implanted wireless microstimulator network with an external wearable wireless hub. (a) Device placement and concept diagram of wireless power and data transmission through intra-cranial networking (b) Microstimulator with the on-chip coil antenna and electrode.

IV. SUB-MILLIMETER WIRELESS MICROSTIMULATORS

Recent stimulators chose to shrink [52]–[57] and lower the power consumption by optimizing the stimulation circumstances. As research on the brain deepened, it became necessary to deal with a broad area of the cortex in a complex manner (as in Fig. 8), and the development of a wireless transceiver was able to support this. The key features are the whole system's on-chip integration and miniaturized wireless power transfer systems using ultrasound (US), inductive, or capacitive coupling. Smaller than invasive surgical tools, these devices only require a simple and non-invasive method to implant into the nervous system.

The tendency of miniaturization, integration, and broad distributions are evident in brain-machine interfaces (BMIs). In 2013, a research team led by Professor Elad Alon and Professor Michel M. Maharbiz of UC Berkeley offered the concept of a distributed neural stimulator, developed a wireless distributed brain signal recording device, and named it Neural Dust [58]. With a microstimulator, three distinguished transceivers are individually located on the skull, the sub-dura, and the IC. The network could connect to peripheral nerves or internal organs to treat or monitor inflammatory diseases. In 2018, the research team at Johns Hopkins University developed a wireless implantable neural stimulation system that applies voltage stimulation according to an external radio signal, named Microbead[54]. The size of the system is incomparably small, which is 0.1mm^3. However, the amount of current obtainable for nerve stimulation is under 100 μA. A research team led by Professor Arto Nurimikko and Professor Yoon-Kyu Song developed a distrusted microstimulator called the optical Neurograin (ONG) and further developed networking methods combined with recording systems [50], [55].

Different approaches have been proposed as the power transmission efficiency (PTE) decreases along with the antenna size in the RF transceiver. The MagNI (Magnetoelectric Neural Implant) used a magnetoelectric

TABLE I. Comparisons of state-of-the-art microstimulators

	Microbead [54]	Stimdust [53]	ONG [50]	MagNI [59]	Charthad, Jayant, et al. [57]
Size	0.3*0.34 mm^3	2.2 mm^3	1.7 × 2.9 mm^2	1.5 mm^2	39 mm^3
Type	Voltage Stim	Current Stim	Current Stim	Current Stim	Current Stim
Current	<40μA	400 μA	25 μA	0.05–1.5 mA	22–5000 μA
Power	RF	US	NIR	magnetoelectric (ME)	US
Target	Cortex	Peripheral	Intracortical	Spinal cord	Peripheral
Tech	130nm RF CMOS	TSMC 65nm LPCMOS	TSMC 180nm RFCMOS	TSMC 180nm CMOS	180nm HV BCD CMOS

transducer to convert an AC magnetic field to AC electrical voltage [59]. Because the lower frequency magnetic field is much stronger without exceeding the safety limits, magnetic fields are chosen based on the simulation data. On the other hand, ultrasonically powered nerve stimulator implants were developed [57]. The implant contains both electrical and optical stimulation sources. Biphasic current stimulation strategies were taken to ensure charge-balanced stimulation. It also implements a robust DL command/data transfer protocol for fully programmable stimulation and a high adaptive voltage (15V) stimulator for chronic applications.

IV. CONCLUSION

This paper described the fundamentals of electroceutical and organized circuit schematics by its purpose. Recent approaches showed state-of-the-art electroceutical focuses on miniaturization and fully integrated wireless interfaces with ultra-low power interfaces. However, there are still hindrances to using these systems directly for clinical trials.

Several elements are combined in the implantable system until it is applied to the human body. In the microstimulator using electrodes, the impedance varies from 8kohm to 11kohm even if the exact specification and process are used. In addition, the efficiency value of the circuit designed in the wireless power receiving circuit, the efficiency measured at the bench top, and the efficiency of the fully integrated system with the antenna and packaging are pretty different. When inserted into a body full of electrolytes, the operating efficiency is often reduced to less than half due to various interferences such as scar tissue, water, or bones. Moreover, design specifications are given tight in the case of a low-power ultra-small system. Other factors that decrease efficiency, as mentioned above, are stimulation rate, mode, the number of electrodes (channels) used, and stimulation pulse parameters vary depending on the subject and disease. Therefore, it is vital to give a sufficient margin because factors decrease efficiency, as mentioned above, when applied to an animal model. Also, adjustment is essential for each patient, even with the same disease. The best way to satisfy both is that the system should have the flexibility and scalability to adapt to different situations. Primarily, a stimulation parameter study optimized for the target disease is essential.

ACKNOWLEDGMENT

The EDA tool was supported by the IC Design Education Center (IDEC), Korea.

REFERENCES

[1] G. Yao *et al.*, “Effective weight control via an implanted self-powered vagus nerve stimulation device,” *Nat. Commun.*, vol. 9, no. 1, pp. 1–10, 2018, doi: 10.1038/s41467-018-07764-z.

[2] T. Izumi *et al.*, “Vagus-macrophage-hepatocyte link promotes post-injury liver regeneration and whole-body survival through hepatic FoxM1 activation,” *Nat. Commun.*, vol. 9, no. 1, pp. 1–13, 2018, doi: 10.1038/s41467-018-07747-0.

[3] P. Chen *et al.*, “Wireless electrical stimulation of the vagus nerves by ultrasound-responsive programmable hydrogel nanogenerators for anti-inflammatory therapy in sepsis,” *Nano Energy*, vol. 89, no. PA, p. 106327, 2021, doi: 10.1016/j.nanoen.2021.106327.

[4] I. T. Mughrabi *et al.*, “Development and characterization of a chronic implant mouse model for vagus nerve stimulation,” *Elife*, vol. 10, pp. 1–24, 2021, doi: 10.7554/ELIFE.61270.

[5] R. H. Howland, “Vagus Nerve Stimulation,” *Curr. Behav. Neurosci. Reports*, vol. 1, no. 2, pp. 64–73, 2014, doi: 10.1007/s40473-014-0010-5.

[6] H. Ulusan, A. Muhtaroglu, and H. Kulah, “A Sub-500 μ W Interface Electronics for Bionic Ears,” *IEEE Access*, vol. 7, pp. 132140–132152, 2019, doi: 10.1109/ACCESS.2019.2940744.

[7] E. With, W. F. Circuit, and A. Muhtaro, “Fully Implantable Cochlear Implant Interface,” vol. 27, no. 7, pp. 1504–1512, 2019.

[8] E. Bloch, Y. Luo, and L. da Cruz, “Advances in retinal prosthesis systems,” *Ther. Adv. Ophthalmol.*, vol. 11, p. 251584141881750, 2019, doi: 10.1177/2515841418817501.

[9] P. Gutruf *et al.*, “Wireless, battery-free, fully implantable multimodal and multisite pacemakers for applications in small animal models,” *Nat. Commun.*, vol. 10, no. 1, 2019, doi: 10.1038/s41467-019-13637-w.

[10] M. S. Khan and H. Deng, “Design and Prototyping a Smart Deep Brain Stimulator: An Autonomous Neuro-Sensing and Stimulating Electrode System,” *IEEE Intell. Syst.*, vol. 32, no. 5, pp. 14–27, 2017, doi: 10.1109/MIS.2017.3711648.

[11] A. Priori, G. Foffani, L. Rossi, and S. Marceglia, “Adaptive deep brain stimulation (aDBS) controlled by local field potential oscillations,” *Exp. Neurol.*, vol. 245, pp. 77–86, 2013, doi: 10.1016/j.expneurol.2012.09.013.

[12] F. A. Koopman *et al.*, “Vagus nerve stimulation inhibits cytokine production and attenuates disease severity in Rheumatoid arthritis,” *Proc. Natl. Acad. Sci. U. S. A.*, vol. 113, no. 29, pp. 8284–8289, 2016, doi: 10.1073/pnas.1605635113.

[13] M. R. Gold *et al.*, “Vagus Nerve Stimulation for the Treatment of Heart Failure: The INOVATE-HF Trial,” *J. Am. Coll. Cardiol.*, vol. 68, no. 2, pp. 149–158, 2016, doi: 10.1016/j.jacc.2016.03.525.

[14] C. C. Horn *et al.*, “Hydrogel-based electrodes for selective cervical vagus nerve stimulation,” *J. Neural Eng.*, vol. 18, no. 5, 2021, doi: 10.1088/1741-2552/abf398.

[15] J. Y. Y. Yap, C. Keatch, E. Lambert, W. Woods, P. R. Stoddart, and T. Kameneva, “Critical Review of Transcutaneous Vagus Nerve Stimulation: Challenges for Translation to Clinical Practice,” *Front. Neurosci.*, vol. 14, no. April, 2020, doi: 10.3389/fnins.2020.00284.

[16] S. Washburn, R. Catlin, K. Bethel, and B. Canlas, “Patient-perceived differences between constant current

and constant voltage spinal cord stimulation systems," *Neuromodulation*, vol. 17, no. 1, pp. 28–36, 2014, doi: 10.1111/ner.12085.

[17] D. S. Kern, A. Fasano, J. A. Thompson, A. Abosch, S. Ojemann, and R. P. Munhoz, "Constant Current versus Constant Voltage: Clinical Evidence Supporting a Fundamental Difference in the Modalities," *Stereotact. Funct. Neurosurg.*, vol. 99, no. 2, pp. 171–175, 2021, doi: 10.1159/000510803

[18] S. Ha, C. Kim, J. Park, G. Cauwenberghs, and P. P. Mercier, "A Fully Integrated RF-Powered Energy-Replenishing Current-Controlled Stimulator," *IEEE Trans. Biomed. Circuits Syst.*, vol. 13, no. 1, pp. 191–202, 2019, doi: 10.1109/TBCAS.2018.2881800.

[19] S. Farahmand, H. Vahedian, M. Abedinkhan Eslami, and A. M. Sodagar, "Wearable, battery-powered, wireless, programmable 8-channel neural stimulator," *Proc. Annu. Int. Conf. IEEE Eng. Med. Biol. Soc. EMBS*, pp. 6120–6123, 2012, doi: 10.1109/EMBC.2012.6347390.

[20] J. Liu, S. Mai, C. Zhang, and Z. Wang, "A High-Voltage, Energy-Efficient, 4-Electrode Output Stage for Implantable Neural Stimulator," *IEEE*, no. 61006022, pp. 762–765, 2015.

[21] W. Ngamkham, M. N. Van Dongen, and W. A. Serdijn, "Biphasic stimulator circuit for a wide range of electrode-tissue impedance dedicated to cochlear implants," *ISCAS 2012 - 2012 IEEE Int. Symp. Circuits Syst.*, pp. 1083–1086, 2012, doi: 10.1109/ISCAS.2012.6271417.

[22] C. Seok *et al.*, "A 16-channel neural stimulator IC with DAC sharing scheme for artificial retinal prostheses," *J. Semicond. Technol. Sci.*, vol. 14, no. 5, pp. 658–665, 2014, doi: 10.5573/JSTS.2014.14.5.658.

[23] R. Shulyzki *et al.*, "320-channel active probe for high-resolution neuromonitoring and responsive neurostimulation," *IEEE Trans. Biomed. Circuits Syst.*, vol. 9, no. 1, pp. 34–49, 2015, [Online]. Available: http://ieeexplore.ieee.org/document/6825915/

[24] K. Abdelhalim and R. Genov, "CMOS DAC-sharing stimulator for neural recording and stimulation arrays," *Proc. - IEEE Int. Symp. Circuits Syst.*, pp. 1712–1715, 2011, doi: 10.1109/ISCAS.2011.5937912.

[25] D. Jiang and A. Demosthenous, "A Multichannel High-Frequency Power-Isolated Neural Stimulator with Crosstalk Reduction," *IEEE Trans. Biomed. Circuits Syst.*, vol. 12, no. 4, pp. 940–953, 2018, doi: 10.1109/TBCAS.2018.2832541.

[26] Y. Wu, D. Jiang, and A. Demosthenous, "A Multi-Channel Stimulator with High-Resolution Time-to-Current Conversion for Vagal-Cardiac Neuromodulation," *IEEE Trans. Biomed. Circuits Syst.*, vol. 15, no. 6, pp. 1186–1195, 2021, doi: 10.1109/TBCAS.2021.3139996.

[27] H. Kassiri, G. Dutta, N. Soltani, C. Liu, Y. Hu, and R. Genov, "An impedance-tracking battery-less arbitrary-waveform neurostimulator with load-adaptive 20V voltage compliance," *Eur. Solid-State Circuits Conf.*, vol. 2016-Octob, pp. 225–228, 2016, doi: 10.1109/ESSCIRC.2016.7598283.

[28] Z. Luo and M. D. Ker, "A High-Voltage-Tolerant and Power-Efficient Stimulator with Adaptive Power Supply Realized in Low-Voltage CMOS Process for Implantable Biomedical Applications," *IEEE J. Emerg. Sel. Top. Circuits Syst.*, vol. 8, no. 2, pp. 178–186, 2018, doi: 10.1109/JETCAS.2018.2796381.

[29] Z. Luo, M.-D. D. M.-D. Ker, T.-Y. Y. T.-Y. Yang, Wan-Hsueh Cheng, W. H. W.-H. Cheng, and Wan-Hsueh Cheng, "A digitally dynamic power supply technique for 16-channel 12 V-tolerant stimulator realized in a 0.18-μm 1.8-V/3.3-V low-voltage CMOS process," *IEEE Trans. Biomed. Circuits Syst.*, vol. 11, no. 5, pp. 1087–1096, Oct. 2017, doi: 10.1109/TBCAS.2017.2713122.

[30] D. Osipov *et al.*, "Current driver with read-out HV protection for neural stimulation," *NORCAS 2016 - 2nd IEEE NORCAS Conf.*, 2016, doi: 10.1109/NORCHIP.2016.7792909.

[31] C.-E. Lee, Y. Jung, and Y.-K. Song, "8-Channel Biphasic Current Stimulator Optimized for Retinal Prostheses.," *J. Nanosci. Nanotechnol.*, vol. 21, no. 8, pp. 4298–4302, 2021, doi: 10.1166/jnn.2021.19405.

[32] D. Zhou, E. Greenbaum, and Eds., *Implantable Neural Prostheses 2: Techniques and Engineering Approaches*. 2010.

[33] D. Osipov *et al.*, "HV compliant current driver with on-chip read-out protection switch for neural stimulation," *Analog Integr. Circuits Signal Process.*, vol. 92, no. 3, pp. 415–426, 2017, doi: 10.1007/s10470-017-1022-3.

[34] X. Li, S. Zhong, and J. Morizio, "16-Channel biphasic current-mode programmable charge balanced neural stimulation," *Biomed. Eng. Online*, vol. 16, no. 1, p. 104, 2017, doi: 10.1186/s12938-017-0385-0.

[35] E. Greenwald *et al.*, "A CMOS Current Steering Neurostimulation Array with Integrated DAC Calibration and Charge Balancing," *IEEE Trans. Biomed. Circuits Syst.*, vol. 11, no. 2, pp. 324–335, 2017, doi: 10.1109/TBCAS.2016.2609854.

[36] Y. J. Jeon, L. Yao, Y. Gao, and M. A. Arasu, "A 0.034% Charge-Imbalanced Neural Stimulation Front-End (SFE) IC with on-Chip Voltage Compliance Monitoring Circuit and Analysis on Resting Potential by Utilizing the SFE IC," *IEEE Trans. Circuits Syst. I Regul. Pap.*, vol. 66, no. 10, pp. 3797–3810, 2019, doi: 10.1109/TCSI.2019.2919333.

[37] Y. Zhou, Z. Wang, K. Wang, and R. Wang, "A Closed-loop Controlled Neural Stimulator with High Voltage Compliance in 0.18-μm Low Voltage CMOS Teachnology," *2019 IEEE Int. Conf. Integr. Circuits, Technol. Appl. ICTA 2019 - Proc.*, no. c, pp. 158–159, 2019, doi: 10.1109/ICTA48799.2019.9012885.

[38] R. Guan, K. M. Emmer, V. Valente, and W. A. Serdijn, "A Power-Efficient and Safe Neural Stimulator Using Ultra-High Frequency Current Pulses for Nerve Conduction Block," *Proc. - APCCAS 2019 2019 IEEE Asia Pacific Conf. Circuits Syst. Innov. CAS Towar. Sustain. Energy Technol. Disrupt.*, pp. 397–400, 2019,

doi: 10.1109/APCCAS47518.2019.8953180.

[39] Y. K. Lo, R. Hill, K. Chen, and W. Liu, "Precision control of pulse widths for charge balancing in functional electrical stimulation," *Int. IEEE/EMBS Conf. Neural Eng. NER*, pp. 1481–1484, 2013, doi: 10.1109/NER.2013.6696225.

[40] W. Y. Hsu and A. Schmid, "Compact, Energy-Efficient High-Frequency Switched Capacitor Neural Stimulator with Active Charge Balancing," *IEEE Trans. Biomed. Circuits Syst.*, vol. 11, no. 4, pp. 878–888, 2017, doi: 10.1109/TBCAS.2017.2694144.

[41] H. Pu, A. R. Danesh, and O. Malekzadeh-arasteh, "A 40V voltage-compliance 12.75 mA maximum-current multipolar neural stimulator using time-based charge balancing technique achieving 2mV precision.," in *IEEE Custom Integrated Circuits Conference (CICC)*, 2021, pp. 3–4.

[42] R. Ranjandish and A. Schmid, "A design methodology for charge-balanced stimulators based on anodic current variation monitoring," *Analog Integr. Circuits Signal Process.*, vol. 101, no. 2, pp. 341–350, 2019, doi: 10.1007/s10470-019-01462-6.

[43] K. Zheng, X. Liu, Z. Qiu, J. Li, W. Wang, and M. Zhang, "Design of a Biphasic Current-Matching Neural Stimulator," *Proc. Int. Conf. Anti-Counterfeiting, Secur. Identification, ASID*, vol. 2019-Octob, pp. 286–290, 2019, doi: 10.1109/ICASID.2019.8925188.

[44] G. O'Leary, D. M. Groppe, T. A. Valiante, N. Verma, and R. Genov, "NURIP: Neural Interface Processor for Brain-State Classification and Programmable-Waveform Neurostimulation," *IEEE J. Solid-State Circuits*, vol. 53, no. 11, pp. 3150–3162, 2018, doi: 10.1109/JSSC.2018.2869579.

[45] C. C. Hsieh and M. D. Ker, "Monopolar Biphasic Stimulator with Discharge Function and Negative Level Shifter for Neuromodulation SoC Integration in Low-Voltage CMOS Process," *IEEE Trans. Biomed. Circuits Syst.*, vol. 15, no. 3, pp. 568–579, 2021, doi: 10.1109/TBCAS.2021.3087036.

[46] J. Y. Son and H. K. Cha, "An Implantable Neural Stimulator IC with Anodic Current Pulse Modulation Based Active Charge Balancing," *IEEE Access*, vol. 8, pp. 136449–136458, 2020, doi: 10.1109/ACCESS.2020.3012028.

[47] B. Lee *et al.*, "An Inductively-Powered Wireless Neural Recording and Stimulation System for Freely-Behaving Animals," *IEEE Trans. Biomed. Circuits Syst.*, vol. 13, no. 2, pp. 413–424, 2019, doi: 10.1109/TBCAS.2019.2891303.

[48] S. Shahdoost, R. J. Nudo, and P. Mohseni, "Generation of Stimulus Triggering From Intracortical Spike Activity for Brain-Machine-Body Interfaces (BMBIs)," *IEEE Trans. Neural Syst. Rehabil. Eng.*, vol. 25, no. 7, pp. 998–1008, 2017, doi: 10.1109/TNSRE.2016.2615270.

[49] S. S. Ghoreishizadeh, D. Haci, Y. Liu, N. Donaldson, and T. G. Constandinou, "Four-Wire Interface ASIC for a Multi-Implant Link," *IEEE Trans. Circuits Syst. I Regul. Pap.*, vol. 64, no. 12, pp. 3056–3067, 2017, doi: 10.1109/TCSI.2017.2731659.

[50] A. H. Lee, J. Lee, J. Jang, A. Nurmikko, and Y. K. Song, "Wireless Addressable Cortical Microstimulators Powered by Near-Infrared Harvesting," *ACS Sensors*, vol. 6, no. 7, pp. 2728–2737, 2021, doi: 10.1021/acssensors.1c00813.

[51] M. Daneshzand, M. Faezipour, and B. D. Barkana, "Robust desynchronization of Parkinson's disease pathological oscillations by frequency modulation of delayed feedback deep brain stimulation," *PLoS One*, vol. 13, no. 11, pp. 1–22, 2018, doi: 10.1371/journal.pone.0207761.

[52] D. Seo *et al.*, "Wireless Recording in the Peripheral Nervous System with Ultrasonic Neural Dust," *Neuron*, vol. 91, no. 3, pp. 529–539, 2016, doi: 10.1016/j.neuron.2016.06.034.

[53] B. C. Johnson *et al.*, "StimDust: A 6.5mm3, wireless ultrasonic peripheral nerve stimulator with 82% peak chip efficiency," in *IEEE Custom Integrated Circuits Conference, CICC*, 2018, pp. 1–4. doi: 10.1109/CICC.2018.8357047.

[54] A. Khalifa *et al.*, "The Microbead: A Highly Miniaturized Wirelessly Powered Implantable Neural Stimulating System," *IEEE Trans. Biomed. Circuits Syst.*, vol. 12, no. 3, pp. 521–531, 2018, doi: 10.1109/TBCAS.2018.2802443.

[55] F. Laiwalla *et al.*, "A Distributed Wireless Network of Implantable Sub-mm Cortical Microstimulators for Brain-Computer Interfaces," *Proc. Annu. Int. Conf. IEEE Eng. Med. Biol. Soc. EMBS*, pp. 6876–6879, 2019, doi: 10.1109/EMBC.2019.8857217.

[56] J. Lee *et al.*, "Neural recording and stimulation using wireless networks of microimplants," *Nat. Electron.*, vol. 4, no. 8, pp. 604–614, 2021, doi: 10.1038/s41928-021-00631-8.

[57] J. Charthad *et al.*, "A mm-Sized wireless implantable device for electrical stimulation of peripheral nerves," *IEEE Trans. Biomed. Circuits Syst.*, vol. 12, no. 2, pp. 257–270, 2018, doi: 10.1109/TBCAS.2018.2799623.

[58] D. Seo, J. M. Carmena, J. M. Rabaey, E. Alon, and M. M. Maharbiz, "Neural Dust: An Ultrasonic, Low Power Solution for Chronic Brain-Machine Interfaces," no. April, 2013, [Online]. Available: http://arxiv.org/abs/1307.2196

[59] Z. Yu *et al.*, "MagNI: A Magnetoelectrically Powered and Controlled Wireless Neurostimulating Implant," *IEEE Trans. Biomed. Circuits Syst.*, vol. 14, no. 6, pp. 1241–1252, Dec. 2020, doi: 10.1109/TBCAS.2020.3037862.

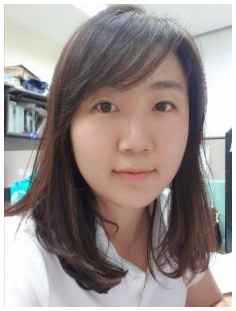

Chae Eun Lee received a BS degree in Electronics Engineering from Ewha Womans University, in 2017 and is currently working toward a Ph.D. degree in Nanoscience and Technology from Seoul National University, Korea.

Her research interests include developing neuromodulation devices for visual prosthesis and bidirectional implantable Brain-Machine Interface.

Yu Ri Kim received a BS degree in Electric Engineering from Soongsil University, Seoul, Korea, in 2018 and is currently working toward Ph. D. degree in Nanoscience and Technology from Seoul National University, Korea.

Her research interests include designing ultra-low-power systems for Brain-Machine Interface and recording Bio-Impedance.

Joon Young Lim received the BS degree in Nanoscience Engineering from Yonsei University, Seoul, Korea, in 2020 and is currently working toward Integrated MS and Ph.D. degree at Seoul National University, Korea.

His main interest is designing and applying machine learning chips in the Brain-Machine Interface system.

Yoon Kyu Song received the BS and MS degree in Electric engineering from Seoul National University, Korea, in 1992 and 1994, respectively, and the Ph.D. degree from Brown University, Providence, RI, in 1999.

His research interests include basic and applied semiconductor optoelectronics, such as vertical-cavity lasers and nanostructured light emitters.